J Biol Inorg Chem (2013) 18:883–893
DOI 10.1007/s00775-013-1033-1

ORIGINAL PAPER

Human anamorsin binds [2Fe–2S] clusters with unique electronic properties

Lucia Banci · Simone Ciofi-Baffoni · Maciej Mikolajczyk · Julia Winkelmann · Eckhard Bill · Maria-Eirini Pandelia

Received: 27 June 2013 / Accepted: 5 August 2013 / Published online: 30 August 2013

Abstract The eukaryotic anamorsin protein family, which has recently been proposed to be part of an electron transfer chain functioning in the early steps of cytosolic iron–sulfur (Fe/S) protein biogenesis, is characterized by a largely unstructured domain (CIAPIN1) containing two conserved cysteine-rich motifs (CX_8CX_2CXC and $CX_2CX_7CX_2C$) whose Fe/S binding properties and electronic structures are not well defined. Here, we found that (1) each motif in human anamorsin is able to bind independently a [2Fe–2S] cluster through its four cysteine residues, the binding of one cluster mutually excluding the binding of the second, (2) the reduced $[2Fe–2S]^{+}$ clusters exhibit a unique electronic structure with considerable anisotropy in their coordination environment, different from that observed in reduced, plant-type and vertebrate-type [2Fe–2S] ferredoxin centers, (3) the reduced cluster bound to the $CX_2CX_7CX_2C$ motif reveals an unprecedented valence localization-to-delocalization transition as a function of temperature, and (4) only the [2Fe–2S] cluster bound to the CX_8CX_2CXC motif is involved in the electron transfer with its physiological protein partner Ndor1. The unique electronic properties of both [2Fe–2S] centers can be interpreted by considering that both cysteine-rich motifs are located in a highly unstructured and flexible protein region, whose local conformational heterogeneity can induce anisotropy in metal coordination. This study contributes to the understanding of the functional role of the CIAPIN1 domain in the anamorsin family, suggesting that only the [2Fe–2S] cluster bound to the CX_8CX_2CXC motif is indispensable in the electron transfer chain assembling cytosolic Fe/S proteins.

Keywords Iron–sulfur cluster · CIAPIN1 domain · Ndor1 · Electron transfer · Mössbauer and EPR spectroscopy

Electronic supplementary material The online version of this article (doi:10.1007/s00775-013-1033-1) contains supplementary material, which is available to authorized users.

L. Banci (✉) · S. Ciofi-Baffoni · M. Mikolajczyk · J. Winkelmann
Magnetic Resonance Center CERM,
University of Florence, Via Luigi Sacconi 6,
50019 Sesto Fiorentino, Florence, Italy
e-mail: banci@cerm.unifi.it

L. Banci · S. Ciofi-Baffoni
Department of Chemistry, University of Florence,
Via della Lastruccia 3,
50019 Sesto Fiorentino, Florence, Italy

E. Bill (✉) · M.-E. Pandelia
Max Planck Institute for Chemical Energy Conversion,
Stiftstr. 34–36, 45470 Mülheim, Germany
e-mail: ebill@gwdg.de

Present Address:
M.-E. Pandelia
Department of Chemistry,
The Pennsylvania State University,
University Park, PA 16802, USA

Introduction

Iron–sulfur (Fe/S) clusters are metallocenters common to a wide variety of proteins, whose functional properties often depend on the electronic structure of these Fe/S cofactors. The most commonly found Fe/S centers include mononuclear [1Fe] centers in rubredoxins, [2Fe–2S] clusters in ferredoxins and Rieske proteins, and [4Fe–4S] clusters in ferredoxins and high-potential Fe/S proteins [1]. Typically, although with exceptions, in all these Fe/S centers the iron

ions are in a tetrahedral coordination environment [2]. Proteins containing the [2Fe–2S] unit are numerous, and several of them are shown to be involved in one-electron-transfer reactions, in which the oxidized $[2Fe–2S]^{2+}$ cluster ($S = 0$ ground state) is reduced to $[2Fe–2S]^{+}$, a deeply valence trapped $Fe^{III}Fe^{II}$ species with an $S = 1/2$ ground state [3]. For [2Fe–2S] ferredoxins of known structure and presumably others as well, one iron atom is closer to the surface (approximately 5 Å), and it has been established by NMR spectroscopy that the added electron resides on this iron [4]. Here, we focused our attention on the human Fe/S binding protein anamorsin, which has recently been proposed to be part of an electron transfer chain functioning in the early steps of cytosolic Fe/S protein biogenesis [5, 6]. The electron transfer process requires the formation of a stable complex with the diflavin reductase Ndor1 [6]. Ndor1 contains a FAD and a FMN prosthetic group and receives electrons from NADPH [7]. This protein consists of two structural domains: the first binds FMN, and the second binds FAD and NADPH [8]. The FMN binding domain (FMN–Ndor1 hereafter) is the part of Ndor1 directly interacting with anamorsin which receives one electron from FMN [6]. Human anamorsin coordinates a [2Fe–2S] cluster through four cysteines arranged in a CX_8CX_2CXC (M1) motif (where X indicates any amino acid) [9]. This motif is a typical feature of the so-called CIAPIN1 domain, located at the C-terminus of more than 300 amino acid sequences of the eukaryotic proteins constituting the anamorsin protein family, which has protein members ranging from basal protozoa to fungi, higher plants and animals, up to humans. All CIAPIN1 domains have an additional well-conserved cysteine-rich $CX_2CX_7CX_2C$ (M2) motif, which forms in vitro two disulfide bonds upon interaction of anamorsin with the oxidoreductase Mia40 [9], an essential protein responsible for protein import and folding in the mitochondrial intermembrane space (IMS) [10–12]. Anamorsin can also be imported into the IMS of isolated mitochondria, where it interacts with Mia40, forming an intermolecular disulfide-bonded intermediate [9]. On the other hand, considering that the chemically reconstituted yeast ortholog of anamorsin, Dre2, has been reported to bind both a [2Fe–2S] cluster and a [4Fe–4S] cluster [5], the M2 motif in anamorsin may also be involved in Fe/S cluster binding. Recent EPR data also support the presence of only [2Fe–2S] clusters in Dre2 when it is isolated from *Escherichia coli* under anaerobic conditions [13]. Besides the members of the anamorsin protein family, no further prokaryotic and eukaryotic non-heme iron binding protein contains the M1 motif or the M2 motif [14–16]. Moreover, since the proteins with the highest pattern similarity to these motifs are involved in coordinating a [2Fe–2S] cluster as well as a [4Fe–4S] cluster, we cannot a priori define whether the two cysteine-rich motifs in anamorsin bind the same or different types of clusters. The Fe/S binding properties of this second, hypothetical cysteine-rich motif are therefore still unclear.

In the present work we have characterized the Fe/S binding properties of both the M1 motif and the M2 motif in human anamorsin through Mössbauer and EPR spectroscopies. We found that both motifs are able to bind a [2Fe–2S] cluster, but only one at a time. The spectroscopic data, once compared with those of reduced $[2Fe–2S]^{+}$ centers of plant-type and vertebrate-type ferredoxins and Rieske proteins, identify a unique electronic structure of the $[2Fe–2S]^{+}$ cluster bound to either the M1 motif or the M2 motif. Furthermore, only the cluster bound to the M1 motif is reduced by the protein partner Ndor1, suggesting that only this cluster participates in the electron transfer chain required for cytosolic Fe/S protein biogenesis.

Materials and methods

Protein production

Mutants of full-length human anamorsin were obtained through site-directed mutagenesis (Agilent QuikChange II site-directed mutagenesis kit) according to the producer's manual, using the Gateway® pEntr-TEV-d-Topo vector containing the sequence coding for the full-length protein as a template. FL, 1-270, and FL-M2 constructs (see "EPR spectroscopy of anamorsin" in the Results section for the meaning of the abbreviations) of human anamorsin were expressed and purified as previously reported [9]. Samples of ^{57}Fe anamorsin (FL and 1–270) were prepared in rich medium following the same procedure, except that an acidic solution of $^{57}Fe^{III}$ was added to the medium at a final concentration of 250 μM. The acidic iron(III) solution was prepared by dissolving $^{57}Fe_2O_3$ in 12 M HCl to a final iron concentration of 125 mM. FMN–Ndor1 (residues 1–174 of the full-length sequence) was expressed and purified as previously reported [6].

EPR spectroscopy

The sample conditions were as follows: protein concentration 200 μM, 50 mM tris(hydroxymethyl)aminomethane (Tris)–HCl pH 8.0, 500 mM NaCl, and 10 % glycerol. Addition of 1 mM sodium dithionite (final concentration in the sample), dissolved in 50 mM Tris–HCl pH 8.0 buffer, and very fast freezing produced the reduced state of the cluster. EPR spectra of oxidized and reduced [2Fe–2S]–anamorsin (FL, 1–270, and FL-M2) were obtained at 45 K using a Bruker Elexsys E500 spectrometer equipped with an X-band microwave bridge (microwave frequency, 9.45 GHz) and a temperature control unit (ER 4131 VT). Experimental baselines were corrected for cavity

contributions by using cubic spine fits. The corrected EPR spectra were simulated with a routine for the calculation of powder spectra with anisotropic g values and angular dependent line widths, using the program ESIM.

Redox chemistry by UV–visible spectroscopy

Protein concentrations of FMN–Ndor1, FL, 1–270, and FL–M2 were measured by UV–visible spectroscopy at 280 nm using molar absorptivities of 20,970, 13,980, 11,000, and 13,980 M^{-1} cm^{-1}, respectively, and/or by Bradford protein assay. Dithionite solution was prepared in an anaerobic chamber with degassed buffer. The dithionite concentration was determined by measuring the absorbance at 315 nm using a molar absorptivity of 6,900 M^{-1} cm^{-1}. FMN–Ndor1 (200 μM) was stepwise reduced to form the fully reduced state ($FMNH_2$–Ndor1) by addition of 1 equiv of dithionite. The $FMNH_2$–Ndor1 form was then mixed with oxidized [2Fe–2S]–anamorsin up to a 2:1 molar ratio (i.e., $FMNH_2$–Ndor1 to FL, or 1–270, or FL–M2). Absorbance changes at 432 nm, the isosbestic point of the $FMNH_2$–Ndor1 and $FMNH^{\cdot}$–Ndor1 species, were monitored for the indicated time period in degassed 300 mM NaCl, 1 mM dithiothreitol, 50 mM phosphate buffer at pH 7.0 in anaerobic conditions using a Cary 50 Eclipse spectrophotometer.

Mössbauer spectroscopy

The sample conditions were as follows: protein concentration 1.2 mM, 50 mM Tris–HCl pH 8.0, 500 mM NaCl, and 5 % glycerol. Reduced samples were obtained with 3 mM sodium dithionite (final concentration in the sample) as reported for the EPR measurements. Mössbauer data were recorded using a spectrometer with alternating constant acceleration. The minimum experimental line width was 0.24 mm s^{-1} (full width at half height). The sample temperature was maintained constant with either an Oxford Instruments Variox or an Oxford Instruments Mössbauer Spectromag cryostat. The latter is a split-pair superconducting magnet system for applied fields up to 8 T where the temperature of the sample can be varied in the range 1.5–250 K. The field at the sample is perpendicular to the γ-beam. The ^{57}Co/Rh source (1.8 GBq) was positioned at room temperature inside the gap of the magnet system at a zero-field position. Isomer shifts are quoted relative to iron metal at 300 K.

Magnetic Mössbauer spectra were simulated with our program MX (by E.B.) by diagonalization of the usual spin Hamiltonian for the spin $S = 1/2$ of the [2Fe–2S] clusters; the hyperfine interactions for both ^{57}Fe sites were calculated by using the usual nuclear Hamiltonian with hyperfine coupling constant given with respect to S [17, 18].

Results

EPR spectroscopy of anamorsin

To investigate the Fe/S binding properties of the cysteine-rich motifs M1 and M2 in human anamorsin, two protein constructs were recombinantly expressed in *E. coli*, namely, the full-length protein (FL), comprising residues 1–312, which include both the M1 motif and the M2 motif, and a construct restricted to residues 1–270, containing only the M1 motif (hitherto called 1–270). Both proteins were isolated from *E. coli* with an Fe/S cluster bound (protein-to-Fe-to-S ratio of 1:1.3:1.3), which is EPR-silent. This is consistent with the presence of either oxidized diferric [2Fe–2S] or mixed-valence [4Fe–4S] clusters, in their diamagnetic (2+) state. Sodium dithionite reduced samples of FL and 1–270 are, in contrast, EPR-active (Fig. 1, spectra a and b, respectively). The EPR spectrum of reduced 1–270 shows three sharp derivative peaks, which can be readily simulated with a single rhombic powder spectrum with principal g values of 2.00, 1.96, and 1.92 (Fig. 1, spectra b, green trace). The average g value ($g_{av} = 1.96$) as well as its anisotropy are characteristic of four-cysteine-ligated $[2Fe–2S]^{+}$ clusters [19], resembling more closely the properties of adrenodoxin [20], which has similarly low anisotropy with g values close to the

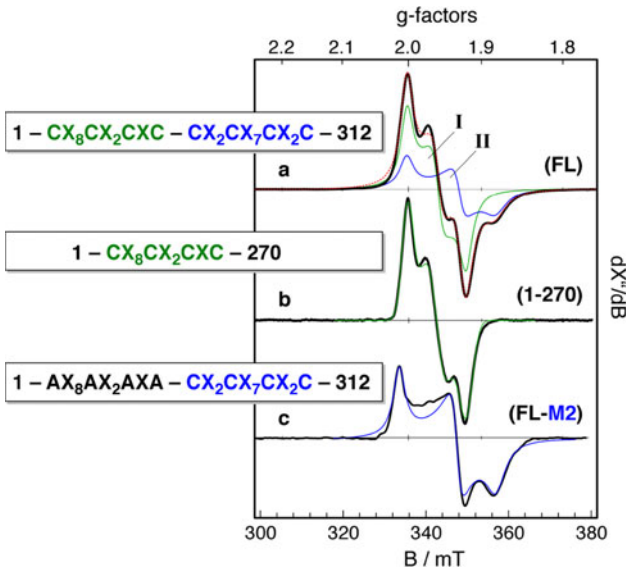

Fig. 1 X-band EPR spectra of reduced [2Fe–2S]–anamorsin. The spectra of FL (*a*), 1–270 (*b*), and FL–M2 (*c*) at 45 K are reported (see the text for the meaning of FL, 1–270, and FL-M2). The *colored lines* are powder simulations with g values given in Table 1; the *red line* is the sum of simulated subspectra I and II. The experimental conditions were as follows: microwave frequency 9.3992 GHz (*a*), 9.3870 GHz (*b*), and 9.4088 GHz (*c*); microwave power 5.2 mW, modulation 0.8 mT (*a*, *c*) and 0.5 mT (*b*)/100 kHz. The labels on the *left* depict the cluster binding motifs for the different protein constructs and mutants investigated in this work

Table 1 EPR g values of reduced [2Fe–2S]–anamorsin constructs in comparison with $[2Fe–2S]^{+}$ clusters in ferredoxins and Rieske protein

	g_{max}	g_{mid}	g_{min}	$\langle g_{av} \rangle$
1–270	2.00	1.96	1.92	1.96
FL, subspectrum I	2.00	1.96	1.92	1.96
FL, subspectrum II	2.00	1.93	1.88	1.94
FL–M2	2.01	1.93	1.88	1.94
Adrenodoxin [20]	2.02	1.94	1.93	1.96
Spinach ferredoxin [39]	2.04	1.95	1.88	1.96
Rieske center [23]	2.02	1.90	1.80	1.91

See the text for the meaning of 1–270, FL and FL-M2

free-electron value (Table 1). The presence of a [2Fe–2S] cluster in 1–270 is in agreement with the previously published electrospray ionization mass spectrometry data and UV–visible spectra [9].

The EPR spectrum of the reduced FL is dominated also by three sharp derivative peaks with g values of 2.00, 1.96, and 1.92, similarly to what is observed in 1–270 (Fig. 1, spectra a, subspectrum I). However, the presence of a second, broader component is discernible particularly from the shoulder at 356 mT, upfield of subspectrum I. The experimental spectrum can be nicely simulated by introducing a second subspectrum (subspectrum II) with a relatively wider split of the g values, their being 2.00, 1.93, and 1.88 (Fig. 1, spectra a, blue trace, 43 % relative integral intensity), thus showing that in the reduced FL two $[2Fe–2S]^{+}$ clusters are present with distinctly different coordination environments.

To further explore the origin of this cluster heterogeneity in FL, we produced a quadruple mutant, in which all four cysteine residues of the M1 motif were mutated to alanines, thus abolishing its ability to bind an Fe/S cluster, whereas the M2 motif is still present and available for Fe/S binding. The EPR spectrum of a reduced sample of this mutant (named FL-M2) exhibits a rhombic set of signals with g values of 2.01, 1.93, and 1.88 (Fig. 1, spectra c, simulation in blue). The features of the spectrum and the g values are strikingly similar to those of subspectrum II in FL (Table 1). We can therefore conclude from the comparison of the EPR spectra of FL, 1–270, and FL–M2 (Fig. 1) that subspectrum I of FL with the narrower g splitting originates from the $[2Fe–2S]^{+}$ cluster bound to the M1 motif, whereas broader subspectrum II can be assigned to the $[2Fe–2S]^{+}$ cluster bound to the M2 motif. The data are summarized in Table 1.

The powder spectrum and the g anisotropy of the EPR spectrum of FL–M2 and subspectrum II found in the EPR spectrum of FL are similar to those of plant-type [2Fe–2S] ferredoxins, i.e., spinach ferredoxin (Table 1), but their g_{av} value (1.94) is slightly lower than the value of 1.96 usually found for the four-cysteine-ligated $[2Fe–2S]^{+}$ clusters in both plant-type and vertebrate-type [2Fe–2S] ferredoxins [21, 22] as well as observed here for the $[2Fe–2S]^{+}$ cluster bound to the M1 motif (Table 1). The g_{av} shift of subspectrum II versus subspectrum I in FL (or of FL–M2 versus 1–270) from 1.94 to 1.96 is determined by the two lowest g values in subspectrum II of FL (or in the spectrum of FL-M2) (g_{mid} and g_{min}, Table 1). A similar, even if much more pronounced, decrease of g_{mid} and g_{min} (Table 1) occurs in the Rieske-type $[2Fe–2S]^{+}$ center, which is coordinated by two cysteine sulfurs and two imidazole nitrogen atoms from histidines [23]. This might suggest the presence, in the M2 motif, of one or two less electron-donating N/O ligands replacing one or two cysteine ligands. However, EPR studies on single cysteine to serine mutants of plant-type and vertebrate-type [2Fe–2S] ferredoxins [21, 22] showed that cysteinyl ligand replacement does not necessarily lead to a decrease in the EPR g_{av} value. Indeed, the relative arrangement of heteroligands and/or the pattern of hydrogen bonds around the cluster are also important determinants of the g_{av} value. Therefore, EPR data alone cannot definitively address whether the [2Fe–2S] cluster bound to the M2 motif is coordinated by the four cysteines of the M2 motif or whether N/O donor ligands substitute some cysteinyl ligands. Mössbauer spectra were therefore acquired to address this issue (see the following sections).

Since electrospray ionization mass spectrometry data indicate the presence of only one [2Fe–2S] unit per protein molecule bound to the CIAPIN1 domain [6], binding of a [2Fe–2S] cluster in one of the two motifs disfavors the binding of a second [2Fe–2S] cluster in the other motif. Consistently, it is not possible to chemically reconstitute the FL protein with both [2Fe–2S] clusters bound at stoichiometric levels; the protein-to-Fe-to-S ratio in reconstituted samples never exceeded 1:2:2 [9]. On the basis of EPR signal intensity ratios derived from the simulations of the EPR spectra of reduced FL, the relative population of the two cluster isomers ranges from 60:40 to 40:60, depending on the sample preparations. In addition, the EPR spectra do not evidence intercluster magnetic interactions, consistent with the binding of a single paramagnetic cluster by only one of the two motifs in a given protein molecule.

Electron transfer between FMN–Ndor1 and [2Fe–2S]–anamorsin

To investigate which of the two [2Fe–2S] clusters bound to anamorsin through the M1 motif or the M2 motif are able to receive electrons from the physiological redox partner Ndor1, we followed the reduction of each individual [2Fe–2S] cluster by Ndor1, following the approach described in [6]. Since [2Fe–2S]–anamorsin interacts with FMN–Ndor1 to receive one electron from the FMN moiety, electron

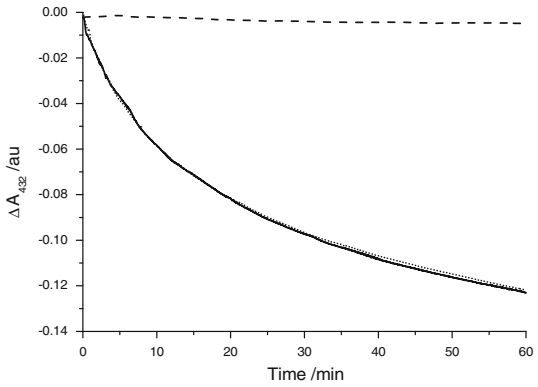

Fig. 2 Electron transfer between [2Fe–2S]–anamorsin and the FMN domain of Ndor1 (FMN–Ndor1). Changes of the absorbance at 432 nm on incubation of reduced FMN–Ndor1 with oxidized [2Fe–2S]–anamorsin (*straight line* FL, *short-dashed line* 1–270, *dashed line* FL–M2). FMN–Ndor1 was first stoichiometrically reduced with sodium dithionite to the fully reduced state $FMNH_2$–Ndor1 and was then mixed with the oxidized [2Fe–2S]–anamorsin (FL, 1–270, and FL–M2) at a 2:1 molar ratio

transfer between FMN–Ndor1 and the various forms of [2Fe–2S]–anamorsin (FL, 1–270, FL–M2) was monitored.

FMN–Ndor1 with the fully reduced state of FMN ($FMNH_2$–Ndor1) was mixed with oxidized FL, or oxidized 1–270, or oxidized FL–M2 in a 2:1 molar ratio, and the one-electron-transfer reaction was followed by UV–visible spectroscopy. The absorbance at 432 nm, i.e., the isosbestic point of the $FMNH_2$–Ndor1 and $FMNH^{\cdot}$–Ndor1 species, decreases over time in the case of FL and 1–270 with the same rates, whereas no changes in absorbance were observed for FL–M2 (Fig. 2). Since the [2Fe–2S] cluster absorbs at 432 nm only in its oxidized state, the data demonstrate that reduction of the [2Fe–2S] cluster occurs only when the latter is bound to the M1 motif. The same behavior was observed for Dre2 chemically reconstituted in its fully metallated state, i.e., containing both a [2Fe–2S] cluster and a [4Fe–4S] cluster per protein, where indeed only the [2Fe–2S] cluster was reduced by the physiological redox partner Tah18, whereas the [4Fe–4S] center is not involved in the electron transfer reaction [5]. In that case, no information is available on how the two clusters are bound to Dre2, i.e., whether, as observed in anamorsin, the two metal binding motifs, M1 and M2, are individually involved in the binding of the two distinct clusters.

Mössbauer spectroscopy of anamorsin

Oxidized anamorsin (1-270 and FL constructs)

The zero-field Mössbauer spectra of oxidized 1–270 show a single well-resolved quadrupole doublet with narrow lines [width (Γ) of 0.30 mm s^{-1}] without paramagnetic broadening or other significant heterogeneity (Fig. 3, upper spectrum). The isomer shift (δ) and electric quadrupole splitting (ΔE_Q), 0.26 and 0.57 mm s^{-1} at 80 K, are typical of high-spin Fe^{III} in a tetrahedral sulfur coordination with four cysteine (RS^-) or sulfide (S^{2-}) ligands [24–27]. Such all-ferric FeS_4 sites are found in mononuclear centers such as in rubredoxin, in four-cysteine-coordinated $[2Fe–2S]^{2+}$ clusters of oxidized ferredoxins, and in oxidized $[3Fe–4S]^{+}$ clusters [25]. The presence of rubredoxin-like Fe^{III} sites ($S = 5/2$) and $[3Fe–4S]^{+}$ clusters ($S = 1/2$) can be ruled out for oxidized 1–270, because the protein is EPR-silent and applied-magnetic-field Mössbauer measurements reveal the presence of a diamagnetic ground state in a partially reduced sample (Fig. S1). Hence, the Fe/S center bound to the M1 motif in the oxidized 1–270 is a four-cysteine-ligated $[2Fe–2S]^{2+}$ cluster with an $S = 0$ ground state.

Oxidized FL shows a zero-field Mössbauer spectrum at 80 K similar to that of oxidized 1–270 (Fig. 3, lower spectrum), but with broader lines. The spectrum can be fitted by two quadrupole doublets, subspectra I and II, with the intensity ratio 57:43 reported in Fig. 3 for the EPR subspectra of reduced FL (approximately 10 % uncertainty). Mössbauer subspectrum I has the same parameters as those found for 1–270, whereas subspectrum II has

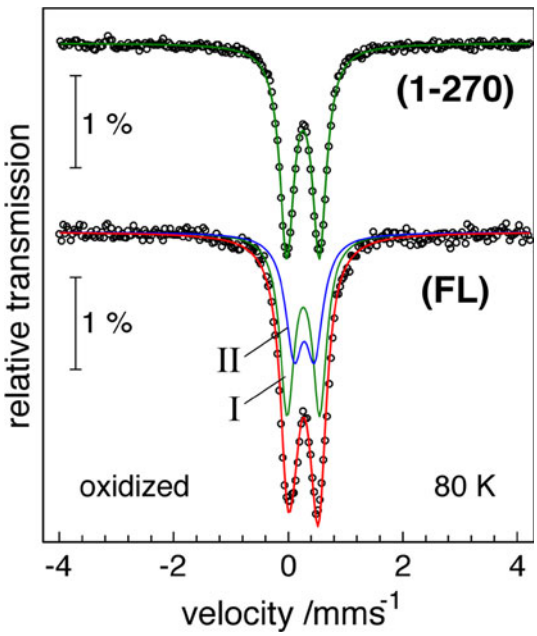

Fig. 3 Zero-field Mössbauer spectra of oxidized [2Fe–2S]–anamorsin. The spectra of 1–270 (*top*) and FL (*bottom*) constructs at 80 K are reported. The *green lines* and the *blue lines* are fits of subspectra I and II with Lorentzian doublets representing the $[2Fe–2S]^{2+}$ clusters bound to the M1 motif and the M2 motif, respectively. The *red line* in the lower spectrum represents the superposition of subspectra I and II with an intensity ratio of 57:43

an isomer shift similar to that found for 1–270 but smaller quadrupole splitting ($\delta = 0.28$ mm s^{-1}, $\Delta E_Q = 0.39$ mm s^{-1} at 80 K). We therefore assign subspectrum I to the Fe/S cluster bound to the M1 motif and subspectrum II to the Fe/S cluster bound to the M2 motif. Given that the oxidized FL sample is diamagnetic, the Mössbauer data of subspectra I and II, being characteristic of ferric irons, confirm that the Fe/S clusters bound to the M1 motif or the M2 motif are both $[2Fe–2S]^{2+}$ clusters, but with slightly different coordination environments, the latter aspect being in agreement with the different EPR g values in reduced FL. For comparison, the oxidized four-cysteine-ligated $[2Fe–2S]^{2+}$ cluster in putidaredoxin has $\delta = 0.27$ mm s^{-1} and $\Delta E_Q = 0.60$ mm s^{-1} at 4.2 K [28], whereas the oxidized two-histidine/two-cysteine-ligated $[2Fe–2S]^{2+}$ cluster in the Rieske protein from *Thermus thermophilus* shows two distinct quadrupole subspectra with $\delta_{1/2} = 0.24/0.32$ mm s^{-1} and $\Delta E_{Q,1/2} = 0.52/0.91$ mm s^{-1} at 4.2 K [23]. In the latter system, the subspectrum with the higher isomer shift represents the two-histidine-coordinated ferric site. Such an extreme situation is not encountered here, neither for subspectrum I nor for subspectrum II of FL. In particular, a large quadrupole splitting is absent in subspectra I and II of FL, at variance with that of the histidine-ligated iron site present in the oxidized Rieske center ($\Delta E_{Q2} = 0.91$ mm s^{-1}) or those in structurally well characterized synthetic diferric model compounds with mixed FeS_4/FeS_2N_2 sites ($\Delta E_{Q,1/2} = 0.49/0.98$ mm s^{-1}, respectively [29]). Relatively large quadrupole splitting is also found for symmetric model compounds with two such $Fe^{III}S_2N_2$ sites with distorted coordination polyhedra (showing identical subspectra with $\Delta E_Q = 0.89–0.97$ mm s^{-1} [30]). The presence of just one histidine ligand (FeS_4/FeS_3N sites) can also be excluded as it has been shown to exert a much greater quadrupole splitting for the respective associated FeS_3N site of the [2Fe–2S] cluster, such as in the cases of the transcription factor IscR ($\Delta E_{Q2} = 0.72$ mm s^{-1} [31]) and Fra2-Grx3 yeast iron regulatory protein ($\Delta E_{Q2} = 0.82$ mm s^{-1} [32]). We presume that such quadrupole splitting should be expected for hypothetical $Fe^{III}S_2O_2$ or $Fe^{III}S_3O$ sites in which similar d-charge anisotropy is caused by the difference in the covalency of Fe–S and Fe–O bonds. The small quadrupole splitting, therefore, excludes the substitution of two (or one) cysteine residues of the $[2Fe–2S]^{2+}$ center in the M2 motif with "hard" N/O donor ligands, whereas it supports more a model where subspectrum II arises from a $[2Fe–2S]^{2+}$ cluster bound by the four cysteines of the M2 motif. In support of this conclusion, the similarity of the isomer shifts between the $[2Fe–2S]^{2+}$ cluster bound to the M2 motif ($\delta = 0.28$ mm s^{-1}) and a four-cysteine-ligated $[2Fe–2S]^{2+}$ cluster ($\delta = 0.27$ mm s^{-1} [33]) is consistent with the absence of N/O–iron ligation, as indeed isomer shifts depend on the nature of the coordinating atom in the order $\delta(S) < \delta(N) < \delta(O)$ [32]. The Mössbauer parameters of the $[2Fe–2S]^{2+}$ clusters in FL are therefore consistent with those observed for a four-cysteine-ligated cluster.

Reduced 1–270 construct of anamorsin

After reduction with sodium dithionite, 1–270 does not show any resolved zero-field Mössbauer spectra in the temperature range 80–220 K. Instead, weak signals are found spread over a large spectral range without any resolved features (Fig. 4, panel a). The origin of this phenomenon cannot be deterioration of the sample, because well-resolved magnetic spectra can be measured at liquid-helium temperatures (Fig. 5, spectra a). Moreover, EPR signals were detected for reduced 1–270, as shown earlier. Therefore, the resonance spreading in the zero-field Mössbauer spectra must arise from strong paramagnetic broadening of the otherwise expected Mössbauer quadrupole doublets. This is due to flipping of the electron spin with intermediate-to-slow relaxation rates relative to the lifetime of the Mössbauer nucleus and the nuclear Larmor precession time of typically 10^{-7} s. Such relaxation broadening is not observed for $[2Fe–2S]^{+}$ clusters of plant-type ferredoxins, which, in contrast, exhibit almost fast spin relaxation at temperatures as low as 80 K and fully resolved pure quadrupole doublets above approximately 160 K [27]. However, a similar intermediate-to-slow electron spin relaxation behavior was observed before for the $[2Fe–2S]^{+}$ clusters in adrenodoxin, a vertebrate-type ferredoxin [27]. It was explained by an electron spin–lattice relaxation time longer than that observed for the $[2Fe–2S]^{+}$ center in plant-type spinach ferredoxin, due to a smaller orbital momentum of the electron spin ground state, consistent with a lower spread of the EPR g values in adrenodoxin with respect to spinach ferredoxin (Table 1). In this respect, the $[2Fe–2S]^{+}$ cluster bound to the M1 motif of 1–270 is also similar to the adrenodoxin cluster (Table 1).

At 4.2 K and with a polarizing field of only 40 mT applied perpendicular to the γ-rays, reduced 1–270 exhibits nicely resolved paramagnetic Mössbauer spectra with large magnetic splitting (Fig. 5, spectra a), revealing complete mitigation of electron spin relaxation and static behavior of the internal magnetic fields experienced by the ^{57}Fe Mössbauer nuclei.

The paramagnetic Mössbauer spectra of 1–270 (Fig. 5, spectra a) were simulated with the usual spin Hamiltonian for dinuclear $Fe^{III}Fe^{II}$ clusters with an $S = 1/2$ ground state with individual components of equal intensity for the two iron sites of the cluster [18, 34], and the Mössbauer parameters specified in Tables 2 and S1 were obtained. A minor diamagnetic subspectrum with 4 % relative intensity was additionally introduced in the simulations to account

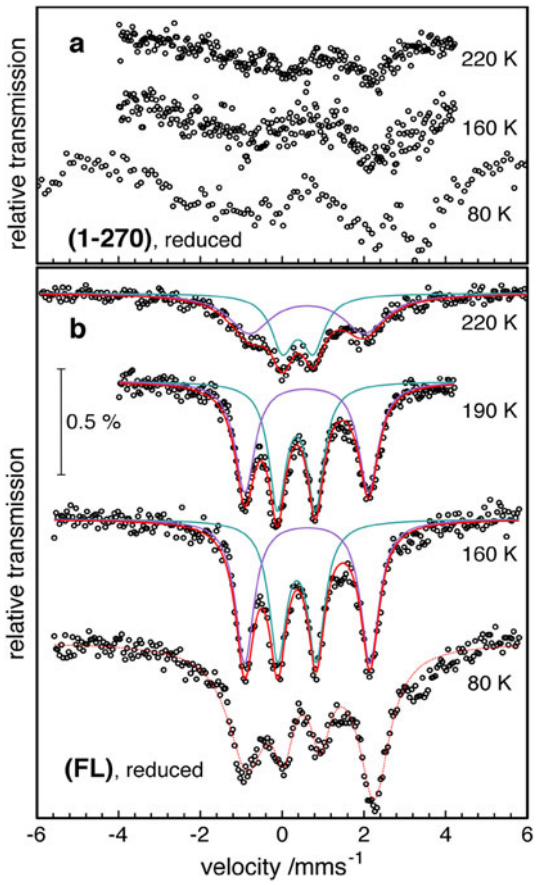

Fig. 4 Zero-field Mössbauer spectra of reduced [2Fe–2S]–anamorsin. The spectra of 1–270 (*a*) and FL (*b*) in the range 80–220 K are reported. The *magenta line* and the *cyan line* in panel *b* represent approximate fits with Lorentzian doublets, essentially for the subspectra of the ferric and ferrous sites of the $[2Fe–2S]^{+}$ cluster bound to the M2 motif only, since the subspectra of the cluster in the M1 motif appear to be broadened virtually beyond detection, like those shown in panel *a*) for 1–270. The 80 K spectrum of FL at the *bottom* of panel *b* could not be reasonably fitted with symmetric Lorentzian doublets of equal intensity; the *red line* is an unconstraint fit, shown to guide the eye

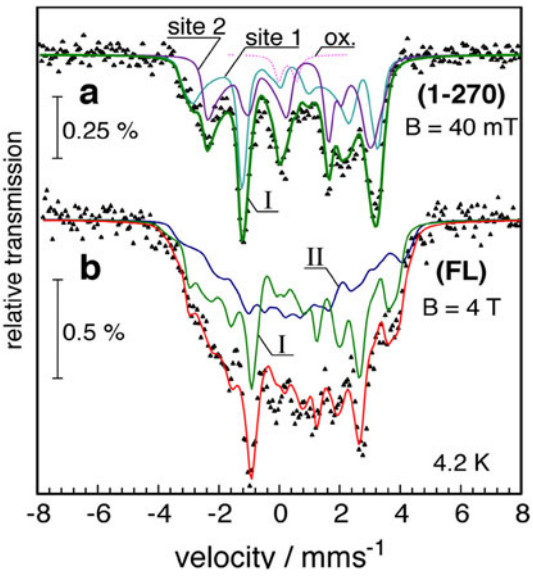

Fig. 5 Magnetic Mössbauer spectra of reduced [2Fe–2S]–anamorsin. The spectra of 1–270 (*a*) and FL (*b*) constructs, recorded at 4.2 K with polarizing fields of 40 mT and 4 T applied perpendicular to the γ-beam, are reported. The *green line* labeled *I* in spectra *a*) and the *green line* and the *blue line* labeled *I* and *II* in spectra *b* result from spin-Hamiltonian simulations as described in the text. The components labeled *site 1* and *site 2* in spectra *a* represent ferric and ferrous ions in a $[2Fe–2S]^{+}$ cluster and are shown in *cyan* and *magenta*, respectively. Corresponding components were used in the calculations for subspectra I and II in spectra *b*. Subspectra I and II represent the two $[2Fe–2S]^{+}$ clusters bound to the M1 motif and the M2 motif with an intensity ratio of 57:43 (taken from EPR measurements). The traces of subspectrum I in spectra *a* and *b* were obtained with identical parameters; their shapes are different only because of the different applied fields. The *dotted pink trace* in spectra *a* shows a 4 % contribution from possibly remaining oxidized clusters

for traces of $[2Fe–2S]^{2+}$ clusters (dotted pink trace in Fig. 5, spectra a). The parameters of this component were taken from a corresponding measurement of a partially reduced sample (Fig. S1); they are virtually identical to those of the oxidized sample. The isomer shift of the ferric site in the $[2Fe–2S]^{+}$ cluster of 1–270 is typical of a ferric ion tetrahedrally coordinated by four sulfur ligands as found in four-cysteine-ligated [2Fe–2S] ferredoxins, such as in the plant-type cluster of putidaredoxin (Table 2). On the other hand, the isomer shift of the ferrous ion in 1–270 is greater than that of the ferrous site in putidaredoxin, the former value being closer to that of the distorted ferrous site in a reduced Rieske center (Table 2). Both iron sites of the reduced $[2Fe–2S]^{+}$ cluster in 1–270 also have remarkably large quadrupole splittings with respect to those of four-cysteine-ligated $[2Fe–2S]^{+}$ clusters (Table 2) [33]. The $S = 1/2$ ground state of the reduced dinuclear clusters arises from antiferromagnetic spin coupling of the valence-localized Fe^{III} ($S_1 = 5/2$) and Fe^{II} ($S_2 = 2$) ions, which is sufficiently strong that distinct α-spin and β-spin populations at the respective ions can be estimated from the spin projections. The experimental values of the magnetic hyperfine coupling tensors **A** in 1–270 (Table S1) reflect this approximation, since the **A** values for the two subspectra have opposite signs, resulting from the spins of the individual ions being parallel and antiparallel to the applied field. The ferric site, with the larger spin, has negative **A**-tensor components as expected, according to the negative intrinsic **A** values for isolated FeS_4 sites due to the strong negative Fermi-contact contribution [17]. In conclusion, the $[2Fe–2S]^{+}$ cluster of 1–270 in the mixed-valence $Fe^{III}Fe^{II}$ oxidation state is valence-localized, as typically observed for reduced [2Fe–2S] clusters in ferredoxins [35].

Table 2 Mössbauer isomer shifts and quadrupole splittings of reduced 1–270 and FL

	δ (mm s^{-1})	$\Delta\delta$[a] (mm s^{-1})	$\lvert\Delta E_Q\rvert$ (mm s^{-1})
1–270; Fe^{III}	**0.35**	–	**0.91**
FL, subspectrum II[b]; Fe^{III}	**0.37**	–	**1.17**
Putidaredoxin; Fe^{III}	0.35	–	0.6
Rieske center; Fe^{III}	0.31	–	0.63
1–270; Fe^{II}	**0.70**	**0.35**	**3.24**
FL, subspectrum II[b]; Fe^{II}	**0.71**	**0.34**	**3.57**
Putidaredoxin; Fe^{II}	0.65	0.30	2.7
Rieske center; Fe^{II}	0.74	0.43	3.05

The values in bold are obtained from simulation of the magnetic spectra recorded at 4.2 K (Figs. 5, S1). For comparison, the corresponding values for putidaredoxin from *Pseudomonas putida* [28] and the Rieske protein from *Thermus thermophilus* are reported [23]. See Table S1 for details

[a] Difference of isomer shifts $\delta(Fe^{II}) - \delta(Fe^{III})$

[b] Only subspectrum II of FL is listed because the parameters for subspectrum I were taken from 1–270

Reduced FL construct

The zero-field Mössbauer spectra of reduced FL measured at 160 and 190 K show two well-resolved quadrupole doublets of equal intensity without much magnetic splitting, as a consequence of fast electron spin relaxation (Fig. 4, panel b). Since the $[2Fe–2S]^+$ cluster in the M1 motif of 1–270 showed extensive broadening in the zero-field Mössbauer spectra (Fig. 4, panel a), we assign the resolved spectra observed for FL to the $[2Fe–2S]^+$ cluster bound to the M2 motif, whereas the spectrum of the $[2Fe–2S]^+$ cluster bound to the M1 motif in FL appears to be broadened virtually beyond detection, as occurs in 1–270. The Mössbauer parameters for the $[2Fe–2S]^+$ cluster bound to the M2 motif are $\delta_1 = 0.37$ mm s^{-1}, $\Delta E_{Q,1} = 0.94$ mm s^{-1} and $\delta_2 = 0.62$ mm s^{-1}, $\Delta E_{Q,2} = 3.07$ mm s^{-1} at 160 K, where the best resolution and sharpest lines were obtained (Table 3). The first component is again typical of a ferric iron tetrahedrally coordinated by four sulfur ligands as found in the four-cysteine-ligated $[2Fe–2S]^+$ cluster of putidaredoxin (Table 2). The other component corresponds to a ferrous iron, characterized by an isomer shift significantly greater than that found in four-cysteine-ligated $[2Fe–2S]^+$ clusters ($\delta = 0.65$ mm s^{-1} at 4.2 K [33]), as found also for 1–270 (Table 2). Both iron sites of the reduced $[2Fe–2S]^+$ cluster in the M2 motif of FL also have remarkably large quadrupole splittings with respect to those of four-cysteine-ligated $[2Fe–2S]^+$ clusters (Table 2) [33].

The magnetic spectrum of reduced FL (Fig. 5, spectra b) shows the presence of two independent clusters (subspectra I and II), roughly with a 57:43 distribution of binding to the M1 motif or the M2 motif (intensities taken from EPR measurements). Reduced FL has a magnetic spectrum that is less resolved than that of 1–270 owing to overlap of a larger number of magnetic lines. The spectrum can be satisfactorily deconvoluted by spin-Hamiltonian simulations as described for reduced 1–270. Half of the spectral intensity (57 %) can be fitted as composed of two components corresponding to the ferric and ferrous sites belonging to one cluster with parameters taken from 1–270 (the two components, once combined, provide the green trace shown in Fig. 5, spectra b as subspectrum I). The remaining half of the intensity (43 %) could be simulated with other two components derived from a ferric iron and a ferrous iron, but with different Mössbauer parameters with respect to those of subspectrum I (the two components,

Table 3 Mössbauer parameters of FL

Temperature (K)	Sample	δ(mm s^{-1})	ΔE_Q(mm s^{-1})	Γ (mm s^{-1})	$\Delta\delta$ (mm s^{-1})
80	FL-I/FL-II[a] (oxidized)	0.26/0.28	0.57/0.39	0.30/0.38	–
4.2	Fe^{III} (reduced)	0.37	1.17	0.26	0.34
	Fe^{II} (reduced)	0.71	3.26	0.26	
160	Fe^{III} (reduced)	0.37	0.94	0.51	0.25
	Fe^{II} (reduced)	0.62	3.07	0.54	
190	Fe^{III} (reduced)	0.35	0.93	0.51	0.25
	Fe^{II} (reduced)	0.60	3.03	0.58	
220	Fe^{III} (reduced)	0.39	0.75	0.66	0.22
	Fe^{II} (reduced)	0.61	2.81	1.26	

The values are obtained from fits of the resolved quadrupole spectra shown in Figs. 3 and 4, panel b with Lorentzian lines. The two values for the parameters of reduced FL refer to Fe^{III} and Fe^{II} ions in the cluster bound to the M2 motif. Γ is the line width and $\Delta\delta$ is the difference of isomer shifts of the "ferrous" and "ferric" ions in the reduced sample

[a] The spectrum of oxidized FL was fitted by a 1:1 sum of two quadrupole doublets (labeled as *FL-I* and *FL-II*), one of which (FL-I) has the parameters found for 1–270. The parameters are reported for both FL-I and FL-II

once combined, provide the blue trace shown in Fig. 5, spectra b as subspectrum II). We assign subspectra I and II to the two $[2Fe\text{-}2S]^{+}$ clusters bound to the M1 motif or the M2 motif of FL, respectively. The Mössbauer parameters are summarized in Tables 2 and S1.

Electron hopping in the $[2Fe–2S]^{+}$ cluster bound to the M2 motif of FL

For a large number of tetrahedral Fe/S complexes, a general empirical relation has been shown to correlate the Mössbauer isomer shift to the oxidation state of iron, i.e., $\delta(x) = (1.4 - 0.4x)$ mm s^{-1}, where x represents an integer or a fractional oxidation number depending on the degree of electron delocalization in Fe/S clusters [36]. Accordingly, localized ferrous and ferric sites should exhibit an isomer shift difference ($\Delta\delta$) of about 0.4 mm s^{-1}. This is relatively close to the value of 0.34 mm s^{-1} found at 4.2 K for both the M1-bound $[2Fe–2S]^{+}$ cluster in 1–270 and the M2-bound $[2Fe–2S]^{+}$ cluster in FL (Tables 2, 3). Other localized $[2Fe–2S]^{+}$ clusters with a spin $S = 1/2$ ground state such as the [2Fe–2S] ferredoxin from wild-type *Clostridium pasteurianum* (0.39 mm s^{-1} [37, 38]) or in the *T. thermophilus* Rieske protein (0.43 mm s^{-1} [23]) show similar differences, whereas the $\Delta\delta$ value reported for putidaredoxin is slightly lower (0.30 mm s^{-1} [28]). At 160 K, however, the difference found for the $[2Fe–2S]^{+}$ cluster bound to the M2 motif reduces to 0.25 mm s^{-1} (Table 3, spectra shown in Fig. 4, panel b). This seems to indicate partial valence delocalization. The hypothesis is supported by the fact that the isomer shift of the ferric site does not decrease with temperature in the range 160–220 K (Table 3), as would be expected for any "isolated" iron with a localized valence state. The temperature invariance is indeed completely against the usual trend of isomer shifts to decrease with temperature owing to the increasing second-order Doppler shift [17]. The observed opposite behavior can only occur if the ferric site gains ferrous character from increasing electron delocalization, caused by either coherent resonance interaction or the onset of incoherent "electron hopping." Support for an incoherent dynamic electron delocalization process in the $[2Fe–2S]^{+}$ cluster bound to the M2 motif of FL is also derived from the line widths of the spectra of reduced FL above 160 K, shown in Fig. 4, panel b. Although the lines are relatively broad throughout, the spectra could be reasonably well approximated by two Lorentzian quadrupole doublets. At higher temperatures of 190 and 220 K, however, the two subspectra increasingly merge together, accompanied by significant line broadening, as can be seen best for the upper trace shown in Fig. 4, panel b. The effective and increasing average of the individual spectral contributions from the two iron sites of the $[2Fe–2S]^{+}$ cluster above approximately 190 K reveals a localization-to-delocalization transition of the merging type [37], likely attributable to electron hopping with rates close to the lifetime of the Mössbauer nucleus and its precession rate (approximately 10^{-7} s).

Discussion

Mössbauer and EPR spectra of human anamorsin show that both the M1 motif and the M2 motif bind independently a [2Fe–2S] cluster through the four cysteines of each motif. The [2Fe–2S] cluster bound to the M1 motif has Mössbauer parameters in its oxidized state and an EPR g_{av} value in its reduced state typical of four-cysteine-ligated [2Fe–2S] clusters occurring in plant-type and vertebrate-type ferredoxins. On the other hand, the $[2Fe–2S]^{+}$ cluster bound to the M2 motif exhibits in its reduced state an EPR g_{av} value of 1.94, slightly lower than that usually found for four-cysteine-ligated $[2Fe–2S]^{+}$ clusters in plant-type and vertebrate-type ferredoxins ($g_{av} = 1.96$) [21, 22]. Although this result might suggest the possible involvement of less-electron-donating N/O ligands in its coordination, the Mössbauer parameters of the $[2Fe–2S]^{2+}$ cluster bound to the M2 motif (Table 3) exclude the involvement of one- or two-histidine coordination (absence of large quadrupole splittings and absence of large isomer shifts expected on S → N ligand substitutions [31–33]). Consistently, no histidine residues are present close to the M2 motif and only one histidine residue is present in the entire CIAPIN1 domain, the third from last residue at the C-terminus. Oxygen coordination can be also excluded as quadrupole splittings and isomer shifts larger than those measured in the Mössbauer spectrum of the oxidized FL are expected to be observed [17, 32].

Although each [2Fe–2S] cluster bound to either the M1 motif or the M2 motif of anamorsin is ligated by four cysteine residues, the Mössbauer parameters of these [2Fe–2S] clusters in their reduced state share some features with the Rieske centers, having a two-histidine/two-cysteine coordination (Table 2). In particular, the simulations of the magnetic Mössbauer spectra at 4.2 K of the reduced [2Fe–2S] clusters in both 1–270 and FL show a high isomer shift of the ferrous sites, $\delta = 0.70$ and 0.71 mm s^{-1} (Table 2), resembling more that of the ferrous site in the Rieske center ($\delta = 0.74$ mm s^{-1} [23]) than that of the ferrous site in the four-cysteine-ligated cluster of [2Fe–2S] ferredoxins ($\delta = 0.65$ mm s^{-1} [28, 38, 39]). Moreover, the ferric and ferrous sites in the $[2Fe–2S]^{+}$ cluster bound to either the M1 motif or the M2 motif are characterized by quadrupole splittings larger than those of [2Fe–2S] ferredoxins [33]. These unusual Mössbauer parameters could be rationalized considering that both cysteine-rich motifs are located in a

highly unstructured and flexible protein region in which the presence of local protein conformational heterogeneity can affect anisotropy in the cluster coordination.

The temperature dependence of the Mössbauer spectra of the [2Fe–2S] cluster bound to the M2 motif differs from the temperature dependences known for typical valence-localized $[2Fe–2S]^{+}$ clusters [24, 25] and reveals a unique valence localization-to-delocalization transition due to electron hopping. Such a localization-to-delocalization transition of the merging type has not been observed in physiological protein-bound [2Fe–2S] clusters, but has been observed only in a few synthetic model compounds with mixed-valence [2Fe–2S] cores [40]. A particular temperature-dependent valence delocalization has also been observed in a cysteine to serine mutated [2Fe–2S] ferredoxin from *C. pasteurianum* [37, 38]. This mutant is composed of a mixture of two species in two spin states, a valence-delocalized high-spin form with $S = 9/2$ ($Fd_{9/2}$) and a valence-localized form with $S = 1/2$ ($Fd_{1/2}$), with the $Fd_{1/2}$ fraction performing a temperature-dependent localization-to-delocalization transition without changing the spin state. It is tempting to assume that, in principle, a similar mechanism for temperature-dependent delocalization is operative in the M2-bound $[2Fe–2S]^{+}$ cluster, except that the electron transfer rates are slower throughout and approach the limit of fast relaxation only beyond 273 K. The key factors determining this different behavior are the strength of the double exchange and the strength of localizing dynamic and static effects imposed by the environment. The protein conformational heterogeneity, responsible for the unusual Mössbauer parameters found for the reduced states of both [2Fe–2S] clusters in human anamorsin, may determine the localization-to-delocalization transition in the M2-bound $[2Fe–2S]^{+}$ cluster in a manner similar to that proposed in *C. pasteurianum* $Fd_{1/2}$ [38]. The molecular basis of the protein conformational effects is, however, different in the two cases, as determined by the substitution of a cysteine ligand with a serine in the well-folded protein scaffold of *C. pasteurianum* $Fd_{1/2}$, whereas it results from the intrinsically unstructured and flexible metal binding M2 region in anamorsin. The assumption that the protein conformational freedom influences valence delocalization in a $[2Fe–2S]^{+}$ cluster correlates with the crucial role proposed for the hydrogen-bond network in this process [4, 41]. Protein conformational heterogeneity is indeed expected to largely affect the stability of the hydrogen-bond network, thus altering valence localization.

From a functional point of view, we identified the [2Fe–2S] cluster bound to the M1 motif as the only one involved in the electron transfer process with its partner protein Ndor1. Although in vitro the M1 and M2 motifs of anamorsin are never both simultaneously occupied by a [2Fe–2S] cluster, likely due to their spatial proximity, in vivo anamorsin might be still able to bind two [2Fe–2S] clusters through the action of specific metallochaperones [42]. In any case, the nonmetallation of the M2 site does not prevent protein–protein recognition with Ndor1 and the electron transfer to the [2Fe–2S] cluster bound to the M1 motif. This suggests that the two cluster sites are functionally independent and that the M2 motif is not essential in the electron transfer process required for cytosolic Fe/S protein biogenesis. The M2 motif has been previously [9] found to modulate the subcellular localization of anamorsin in the IMS, being imported through the mitochondrial Mia40-dependent disulfide relay system [10, 11, 43, 44]. In such a process, anamorsin is trapped in the IMS through the oxidoreductase Mia40, which specifically forms two disulfide bonds in the M2 motif. On the other hand, we found here that the M2 motif can also bind a [2Fe–2S] cluster. Considering that anamorsin traffics between the cytoplasm and the nucleus [45] and is involved in intracellular antiapoptotic signaling pathways [46], the [2Fe–2S] cluster bound to the M2 motif might play a regulatory role in these processes. Indeed, besides the electron transfer function, Fe/S clusters are known to function as signaling and regulating agents because of their tunable sensitivity to various oxidants or reductants [47].

Concluding remarks

The CIAPIN1 domain, which is typically present at the C-terminus of the anamorsin protein family, has rather unique properties as it is largely unstructured and contains two fully conserved cysteine-rich motifs, M1 and M2, whose Fe/S binding properties and electronic structures have not been well defined. In this work, we have fully characterized the Fe/S cluster binding properties of both motifs in human anamorsin, demonstrating that the two motifs independently bind a [2Fe–2S] cluster through the four conserved cysteines of each motif, in a mutually exclusive manner. The investigation of their electronic structures shows that, in the reduced state, they have a unique electronic structure with considerable anisotropy in the coordination environment, in contrast to plant-type and vertebrate-type reduced [2Fe–2S] ferredoxin centers. The reduced cluster bound to the M2 motif reveals an unprecedented valence localization-to-delocalization transition due to the onset of electron hopping. All these unique effects can be rationalized by considering that both cysteine-rich motifs, at variance with what is observed for plant-type and vertebrate-type [2Fe–2S] ferredoxins, are located in a highly unstructured and flexible protein region in which local protein conformational heterogeneity affects the cluster coordination. We also found that in vitro only

the [2Fe–2S] cluster bound to the M1 motif is involved in the electron transfer process with its physiological partner protein Ndor1, suggesting that also in vivo only this cluster participates in the electron transfer chain required for cytosolic Fe/S protein biogenesis. In summary, this study delineates the structural and functional role of the metallocofactors in the CIAPIN1 domain of the eukaryotic anamorsin protein family, unequivocally showing that these are [2Fe–2S] clusters with electronic structures rather different from those of known protein-bound [2Fe–2S] clusters.

Acknowledgments We thank Angelo Gallo (CERM) for assistance in recording the EPR spectra and Bernd Mienert for recording the Mössbauer spectra. PRIN (2009FAKHZT_001), BIO-NMR (contract no. 261863), MIUR-FIRB PROTEOMICA (RBRN07BMCT), and Ente Cassa di Risparmio are gratefully acknowledged for financial support. This work was also supported by the European Integrated Structural Biology Infrastructure (Instruct), which is part of the European Strategy Forum on Research Infrastructures and is supported by national member subscriptions. Specifically, we thank the Instruct Core Center CERM (Italy).

References

1. Beinert H (2000) J Biol Inorg Chem 5:2–15
2. Sticht H, Rosch P (1998) Prog Biophys Mol Biol 70:95–136
3. Banci L, Bertini I, Luchinat C (1990) Struct Bond 72:113–135
4. Dugad LB, La Mar GN, Banci L, Bertini I (1990) Biochemistry 29:2263–2271
5. Netz DJ, Stumpfig M, Dore C, Muhlenhoff U, Pierik AJ, Lill R (2010) Nat Chem Biol 6:758–765
6. Banci L, Bertini I, Calderone V, Ciofi-Baffoni S, Giachetti A, Jaiswal D, Mikolajczyk M, Piccioli M, Winkelmann J (2013) Proc Natl Acad Sci USA 110:7136–7141
7. Finn RD, Basran J, Roitel O, Wolf CR, Munro AW, Paine MJ, Scrutton NS (2003) Eur J Biochem 270:1164–1175
8. Murataliev MB, Feyereisen R, Walker FA (2004) Biochim Biophys Acta 1698:1–26
9. Banci L, Bertini I, Ciofi-Baffoni S, Boscaro F, Chatzi A, Mikolajczyk M, Tokatlidis K, Winkelmann J (2011) Chem Biol 18:794–804
10. Banci L, Bertini I, Cefaro C, Ciofi-Baffoni S, Gallo A, Martinelli M, Sideris DP, Katrakili N, Tokatlidis K (2009) Nat Struct Mol Biol 16:198–206
11. Banci L, Bertini I, Cefaro C, Cenacchi L, Ciofi-Baffoni S, Felli IC, Gallo A, Gonnelli L, Luchinat E, Sideris DP, Tokatlidis K (2010) Proc Natl Acad Sci USA 107:20190–20195
12. Sideris DP, Petrakis N, Katrakili N, Mikropoulou D, Gallo A, Ciofi-Baffoni S, Banci L, Bertini I, Tokatlidis K (2009) J Cell Biol 187:1007–1022
13. Soler N, Craescu CT, Gallay J, Frapart YM, Mansuy D, Raynal B, Baldacci G, Pastore A, Huang ME, Vernis L (2012) FEBS J 279:2108–2119
14. Andreini C, Bertini I, Cavallaro G, Najmanovich RJ, Thornton JM (2009) J Mol Biol 388:356–380
15. Andreini C, Banci L, Bertini I, Elmi S, Rosato A (2007) Proteins 67:317–324
16. Bertini I, Luchinat C, Provenzani A, Rosato A, Vasos PR (2002) Proteins Struct Funct Genet 46:110–127
17. Gutlich P, Bill E, Trautwein AX (2011) Mössbauer spectroscopy and transition metal chemistry. Springer, Berlin
18. Trautwein AX, Bill E, Bominaar EL, Winkler H (1991) Struct Bond 78:1
19. Bertrand P, Guigliarelli B, More C (1991) New J Chem 15:445–454
20. Palmer G, Brintzinger H, Estabrook RW (1967) Biochemistry 6:1658–1664
21. Cheng H, Xia B, Reed GH, Markley JL (1994) Biochemistry 33:3155–3164
22. Xia B, Cheng H, Bandarian V, Reed GH, Markley JL (1996) Biochemistry 35:9488–9495
23. Fee JA, Findling KL, Yoshida T, Hille R, Tarr GE, Hearshen DO, Dunham WR, Day EP, Kent TA, Munck E (1984) J Biol Chem 259:124–133
24. Dunham WR, Bearden AJ, Salmeen I, Palmer G, Sands RH, Orme-Johnson WH, Beinert H (1971) Biochim Biophys Acta 253:134–152
25. Beinert H, Holm RH, Munck E (1997) Science 277:653–659
26. Venkateswara Rao P, Holm RH (2004) Chem Rev 104:527–559
27. Cammack R, Rao KK, Hall DO, Johnson CE (1971) Biochem J 125:849–856
28. Munk E, Debrunner PG, Tsibris JCM, Gunsalus IC (1972) Biochemistry 11:863–885
29. Ballmann J, Albers A, Demeshko S, Dechert S, Bill E, Bothe E, Ryde U, Meyer F (2008) Angew Chem Int Ed 47:9537–9541
30. Ballmann J, Sun X, Dechert S, Bill E, Meyer F (2007) J Inorg Biochem 101:305–312
31. Fleischhacker AS, Stubna A, Hsueh KL, Guo Y, Teter SJ, Rose JC, Brunold TC, Markley JL, Munck E, Kiley PJ (2012) Biochemistry 51:4453–4462
32. Li H, Mapolelo DT, Dingra NN, Naik SG, Lees NS, Hoffman BM, Riggs-Gelasco PJ, Huynh BH, Johnson MK, Outten CE (2009) Biochemistry 48:9569–9581
33. Meyer J, Clay MD, Johnson MK, Stubna A, Munck E, Higgins C, Wittung-Stafshede P (2002) Biochemistry 41:3096–3108
34. Schünemann V, Winkler H (2000) Rep Prog Phys 63:263
35. Solomon EI, Randall DW, Glaser T (2000) Coord Chem Rev 200:595–632
36. Hoggins JT, Steinfink H (1976) Inorg Chem 15:1682–1685
37. Achim C, Golinelli M-P, Bominaar EL, Meyer J, Munck E (1996) J Am Chem Soc 118:8168–8169
38. Achim C, Bominaar EL, Meyer J, Peterson J, Munck E (1999) J Am Chem Soc 121:3704–3714
39. Rao KK, Cammack R, Hall DO, Johnson CE (1971) Biochem J 122:257–265
40. Albers A, Demeshko S, Dechert S, Bill E, Bothe E, Meyer F (2011) Angew Chem Int Ed 50:9191–9194
41. Skjeldal L, Markley JL, Coghlan VM, Vickery LE (1991) Biochemistry 30:9078–9083
42. Muhlenhoff U, Molik S, Godoy JR, Uzarska MA, Richter N, Seubert A, Zhang Y, Stubbe J, Pierrel F, Herrero E, Lillig CH, Lill R (2010) Cell Metab 12:373–385
43. Banci L, Bertini I, Calderone V, Cefaro C, Ciofi-Baffoni S, Gallo A, Tokatlidis K (2012) J Am Chem Soc 134:1442–1445
44. Banci L, Bertini I, Calderone V, Cefaro C, Ciofi-Baffoni S, Gallo A, Kallergi E, Lionaki E, Pozidis C, Tokatlidis K (2011) Proc Natl Acad Sci USA 108:4811–4816
45. Park KA, Yun N, Shin DI, Choi SY, Kim H, Kim WK, Kanakura Y, Shibayama H, Oh YJ (2011) J Neural Transm 118:433–444
46. Saito Y, Shibayama H, Tanaka H, Tanimura A, Kanakura Y (2011) Biochem Biophys Res Commun 405:303–307
47. Crack JC, Green J, Thomson AJ, Le Brun NE (2012) Curr Opin Chem Biol 16:35–44